Simulation of the 1976/77 Climate Transition over the North Pacific: Sensitivity to Tropical Forcing

CLARA DESER AND ADAM S. PHILLIPS

National Center for Atmospheric Research, Boulder, Colorado

ABSTRACT

This study examines the contribution of tropical sea surface temperature (SST) forcing to the 1976/77 climate transition of the winter atmospheric circulation over the North Pacific using a combined observational and modeling approach. The National Center for Atmospheric Research (NCAR) Community Atmospheric Model version 3 (CAM3) simulates approximately 75% of the observed 4-hPa deepening of the wintertime Aleutian low from 1950–76 to 1977–2000 when forced with the observed evolution of tropical SSTs in a 10-member ensemble average. This response is driven by precipitation increases over the western half of the equatorial Pacific Ocean. In contrast, the NCAR Community Climate Model version 3 (CCM3), the predecessor to CAM3, simulates no significant change in the strength of the Aleutian low when forced with the same tropical SSTs in a 12-member ensemble average. The lack of response in CCM3 is traced to an erroneously large precipitation increase over the tropical Indian Ocean whose dynamical impact is to weaken the Aleutian low; this, when combined with the response to rainfall increases over the western and central equatorial Pacific, results in near-zero net change in the strength of the Aleutian low. The observed distribution of tropical precipitation anomalies associated with the 1976/77 transition, estimated from a combination of direct measurements at land stations and indirect information from surface marine cloudiness and wind divergence fields, supports the models' simulated rainfall increases over the western half of the Pacific but not the magnitude of CCM3's rainfall increase over the Indian Ocean.

---

1. Introduction

The wintertime atmospheric circulation over the North Pacific has undergone a substantial long-term intensification since the late 1940s (Nitta and Yamada 1989; Trenberth 1990; Trenberth and Hurrell 1994; Mantua et al. 1997; Minobe 1997; Zhang et al. 1997; Deser et al. 2004; among others). This intensification, manifest as a deepening of the climatological Aleutian low pressure system, is responsible for widespread climatic changes over North America (Cayan et al. 2001; Dettinger et al. 2000) and physical and biological changes within the North Pacific Ocean (Miller et al. 1994; Deser et al. 1996; Mantua et al. 1997; Deser et al. 1999; Miller et al. 1998). Because of its relatively rapid onset in the late 1970s, this long-term circulation variation has been termed the "1976/77 climate transition" (Nitta and Yamada 1989; Trenberth 1990; Miller et al.

1994; Graham et al. 1994). A similar long-term deepening of the Aleutian low occurred during the first half of the twentieth century, followed by a strengthening (Minobe 1997; Zhang et al. 1997; Deser et al. 2004).

The current view of the origin of the North Pacific 1976/77 climate transition is that it was initiated by changes in tropical sea surface temperatures (SSTs) over the Pacific and Indian Ocean sectors (Minobe 1997; Graham et al. 1994; Zhang et al. 1997; Deser et al. 2004). Since 1977, tropical SSTs have increased by approximately 0.4°C over the Indian Ocean and far western Pacific and by approximately 0.6°C over the eastern Pacific relative to the period 1950–76 (Fig. 1). This pattern of SST change is similar to that which occurs during the warm phase of the El Nino–Southern Oscillation (ENSO) phenomenon, although the Indian Ocean SST increases are relatively more prominent and the eastern Pacific SST changes are not narrowly confined to the equatorial upwelling zone (Garreaud and Battisti 1999; Deser et al. 2004). The proposed mechanism for the 1976/77 climate transition over the North Pacific is similar to that which occurs on interannual time scales in association with ENSO, namely, that tropical Indo-

Corresponding author address: Dr. Clara Deser, Climate and Global Dynamics Division, NCAR, P.O. Box 3000, Boulder, CO 80307-3000.
E-mail: cdeser@ucar.edu

Epoch Difference: 1977-2000 minus 1950-1976

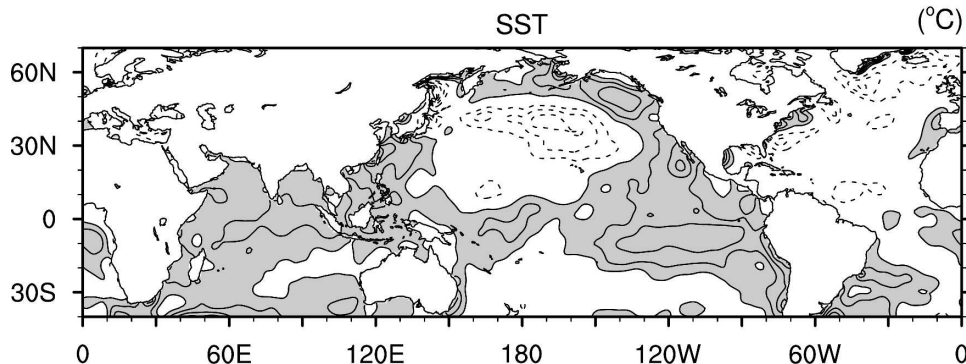SST   (°C)

FIG. 1. Epoch difference map of observed winter (December–February) SST, obtained by subtracting the period 1950–76 from the period 1977–2000, based on the HadISST dataset (Rayner et al. 2003). The contour interval is 0.2°C, negative contours are dashed, and the zero contour is omitted; values >0.2°C are shaded.

Pacific SST anomalies give rise to precipitation anomalies whose associated diabatic heating forces an atmospheric Rossby wave train to the North Pacific (Horel and Wallace 1981) that is subsequently modified by interactions with transient eddies along the North Pacific storm track (Trenberth et al. 1998; Barsugli and Sardeshmukh 2002). As emphasized by DeWeaver and Nigam (2004) with regard to ENSO events, it is the full two-dimensional distribution of tropical rainfall anomalies (both positive and negative) that ultimately determines the pattern and amplitude of the extratropical atmospheric response.

The hypothesis of tropical SST forcing of the 1976/77 climate transition over the North Pacific has been tested to some degree in experiments with atmospheric general circulation models (GCMs) (Chen et al. 1992; Graham 1994; Graham et al. 1994). The results of these early studies generally support the notion that tropical SST forcing plays an important role in the deepening of the Aleutian low since 1977. However, these early investigations contain shortcomings, including the relatively coarse model resolution, limited period of simulation, idealized SST forcing configuration, and single-member integrations. In this study, we make use of a multimember ensemble of integrations with three state-of-the-art atmospheric GCMs forced by the observed history of SSTs over the tropical oceans (20°S–20°N) during the period 1950–2000 to more comprehensively examine the contribution of tropical forcing to the 1976/77 climate transition over the North Pacific.

One difficulty in assessing the role of the Tropics is the lack of adequate rainfall data needed to characterize the full spatial pattern of the tropical precipitation anomalies associated with the 1976/77 transition. Be-fore the advent of satellite rainfall measurements in the mid-1970s, our knowledge of rainfall variability was limited to land stations, leaving vast areas of the tropical oceans unsampled. Recently, studies have demonstrated the utility of ship-based observations of cloud cover and surface wind divergence (see Deser et al. 2004 and Norris 2005) as proxy measures of rainfall over the tropical oceans. We adopt this novel approach to estimate the full spatial pattern of the tropical rainfall changes associated with the 1976/77 climate transition. This approach allows us to assess the realism of the precipitation responses in the atmospheric GCMs forced with observed tropical SSTs, experiments we use to evaluate the role of tropical forcing in the intensification of the Aleutian low since 1950.

The paper is structured as follows. Section 2 describes the observational datasets, atmospheric GCM experiments, and analysis methods. Section 3 describes the results, and section 4 provides a summary and discussion.

2. Data, methods, and model integrations

a. Data

The following monthly averaged observational datasets, available from http://www.cgd.ucar.edu/cas/guide/, have been used in this study; we have analyzed the period of record 1950–2000 unless stated otherwise.

1) Sea level pressure (SLP) from an updated version of Trenberth and Paolino (1980). This archive is based upon daily historical analyses for the Northern Hemisphere poleward of 20°N on a 5° latitude × 5° longitude grid, updated with data from the National

Centers for Environmental Prediction–National Center for Atmospheric Research (NCEP–NCAR) 40-Yr Reanalysis Project (Kalnay et al. 1996).

2) 500-hPa geopotential height from the NCEP–NCAR reanalysis on a 2.5° latitude × 2.5° longitude grid (Kalnay et al. 1996).

3) Land station precipitation from the University of East Anglia's Climate Research Unit (Hulme et al. 1998) on a 2.5° latitude × 3.75° longitude grid, and from Dai et al. (1997) on a 2.5° latitude × 2.5° longitude grid. The last year available is 1998 from Hulme et al. and 1996 from Dai et al.

4) Total cloud amount and surface wind from the International Comprehensive Ocean–Atmosphere Data Set (ICOADS; Woodruff et al. 1987; Worley et al. 2005; Woodruff et al. 2005) on a 2° latitude × 2° longitude grid.

5) SST from the Hadley Centre Sea-Ice and Sea Surface Temperature (HadISST) (Rayner et al. 2003) on a 1° latitude × 1° longitude grid.

b. Methods

We formed monthly anomalies by subtracting the long-term monthly means from each calendar month. Winter (December–February) means were computed from the monthly anomalies. We use simple differences between means for the periods 1950–76 and 1977–2000 to characterize the changes during the second half of the twentieth century; however, linear trends based on the full period of record (1950–2000) give nearly identical results (not shown). For the observational archives that contain substantial amounts of missing data [e.g., station precipitation fields of Hulme et al. (1998) and Dai et al. (1997), and the ICOADS], a minimum of 25% of the winters in each period were required to have data at a given grid box; otherwise, the period mean for that grid box was set to missing. To improve the readability of the ICOADS cloudiness and surface wind divergence epoch difference maps, linear interpolation (across gaps not exceeding 5 points in longitude and 3 points in latitude) and weighted binomial smoothing (9 points in longitude and 3 points in latitude) were applied. The statistical significance of the epoch difference values was assessed by means of Student's t test taking into account serial correlation (Zwiers and von Storch 1995).

Changes in observing practice and instrumentation have caused spurious increases in scalar wind speed and cloudiness since 1950 from the ICOADS (Ward and Hoskins 1996; Norris 1999; Wu and Xie 2003; Norris 2005). Following the recommendations of Norris (2005), we account for these spurious trends by removing the tropical (30°N–30°S) mean cloud amount from each grid box in each winter, and by removing a 4.7% per decade linear trend from the surface zonal and meridional wind components. These "corrections" are not critical to the results shown in this study (i.e., we have compared results with and without the corrections and find only minor differences between them).

c. Model integrations

Integrations with three state-of-the-art atmospheric general circulation models forced by observed monthly SSTs over the tropical oceans (20°N–20°S) during 1950–2000 from the dataset of Hurrell et al. (2005, manuscript submitted to *J. Climate*) are analyzed in this study. These consist of a 12-member ensemble of the National Center for Atmospheric Research Community Climate Model version 3 (CCM3) at T42 horizontal resolution (equivalent to 2.8° latitude × 2.8° longitude), a five-member ensemble of Community Atmosphere Model Version 3 (CAM3) at T42 resolution, and a five-member ensemble of CAM3 at T85 resolution (equivalent to 1.4° latitude × 1.4° longitude). Details of the physical and numerical methods used in CCM3 and CAM3 are provided in Kiehl et al. (1998) and Collins et al. (2006), respectively. The members of the ensemble for each model differ only in their initial conditions. Atmospheric greenhouse gas concentrations are kept fixed throughout the integrations at their 1990 levels. We shall refer to these integrations as "TOGA" (Tropical Ocean–Global Atmosphere) simulations following convention. Each model simulation was forced by the observed history of monthly SSTs in the Tropics (20°N–20°S) and climatological monthly mean SSTs poleward of 30°; a linear transition was used between 20° and 30°.

In addition to the model experiments described above, we have also analyzed the output of a 20-member ensemble of CCM3 integrations forced with the observed linear SST trends over the tropical Indian Ocean conducted by Hoerling et al. (2004); the reader is referred to that paper for details.

3. Results

The change in winter SLP from 1950–76 to 1977–2000 over the North Pacific and adjacent continents is shown in Fig. 2 (left) from observations and the three different TOGA simulations: CCM3, CAM3 (T42), and CAM3 (T85). The model results are based upon the ensemble mean response of 5 (12) TOGA simulations of CAM3 (CCM3). In nature, there is a significant lowering of SLP over the North Pacific during 1977–2000 relative to 1950–1976, with maximum amplitude ~4.5 hPa near the southern tip of the Aleutian Islands. Both CAM3 ensembles simulate a substantial portion of the observed

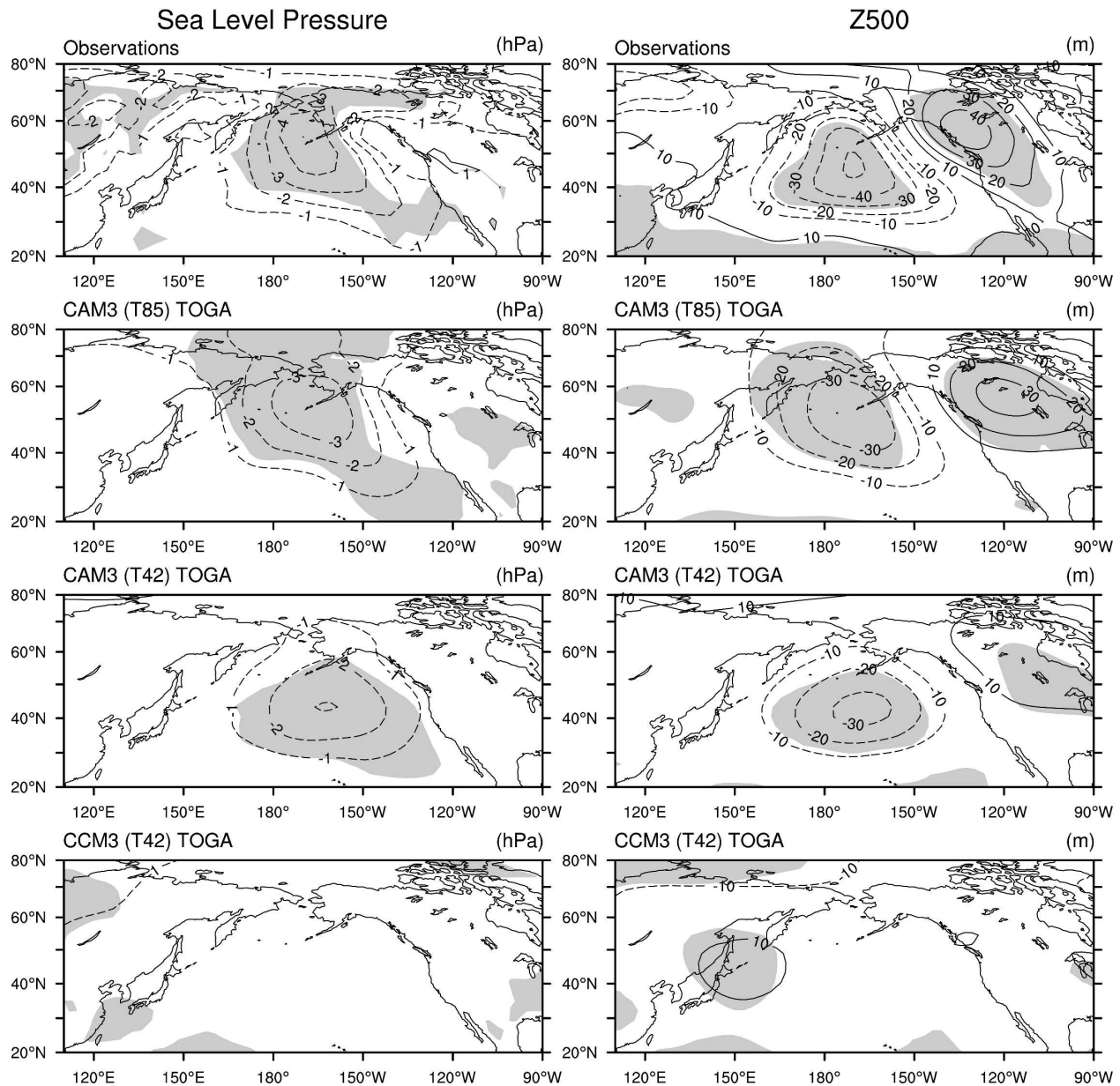## Epoch Differences: 1977-2000 minus 1950-1976

FIG. 2. Epoch differences of winter (December–February) (left) sea level pressure (SLP; left) and (right) 500-hPa geopotential height (Z500), obtained by subtracting the period 1950–76 from the period 1977–2000, from observations and three atmospheric general circulation models forced with observed time-varying tropical sea surface temperatures (referred to as "TOGA" simulations): CAM3 at T85 horizontal resolution, CAM3 at T42 horizontal resolution, and CCM3 at T42 horizontal resolution. The contour interval for SLP (Z500) is 1 hPa (10 m), the zero contours are omitted, negative contours are dashed, and the shading indicates epoch difference values that are statistically significant at the 95% level based on a Student's t test.

signal, with maximum amplitude ~3.5 hPa in the T85 version compared to ~3 hPa in the T42 version; these responses are significant at the 95% level. In contrast to CAM3, the CCM3 TOGA ensemble exhibits near-zero SLP change over the North Pacific and adjacent continents. The 500-hPa geopotential height epoch differ-

ences (Fig. 2, right) exhibit significant negative anomalies over the North Pacific and positive anomalies downstream over western Canada in both nature and the CAM3 simulations (as with SLP, the CAM3 responses are weaker than observed, with maximum negative anomalies ~50 m in observations compared to
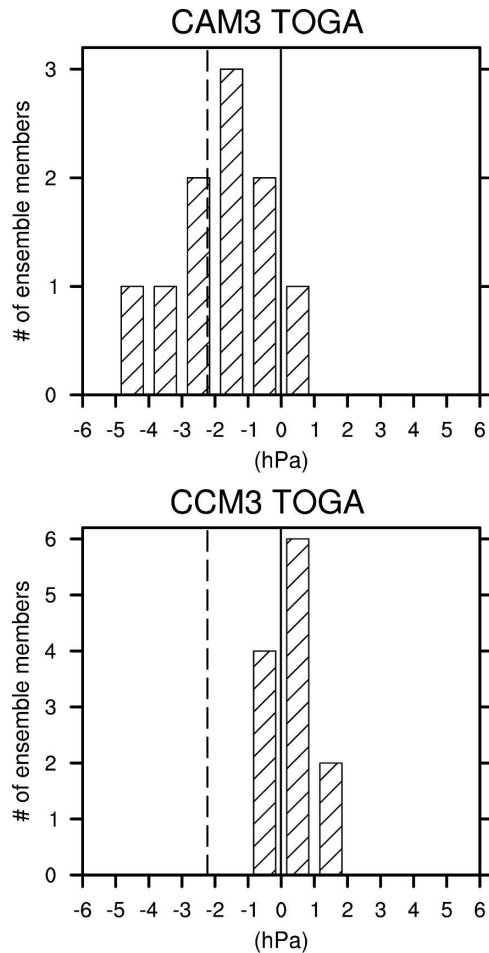
FIG. 3. Histogram of the area-averaged SLP epoch difference response over the North Pacific (30°–65°N, 140°E–160°W) based on the (top) 10 CAM3 TOGA integrations (T42 and T85 combined) and the (bottom) 12 CCM3 TOGA integrations. The dashed vertical line indicates the observed value (−2.24 hPa).

~35 m in CAM3 T85 and ~30 m in CAM3 T42). In contrast to CAM3 and similar to the results for SLP, the CCM3 TOGA ensemble exhibits near-zero height changes over the North Pacific and adjacent continents.

An indication of the spread of the epoch difference response among the individual ensemble members is given in Fig. 3, which shows a histogram of the area-averaged SLP response over the domain 30°–65°N, 140°E–160°W (also known as the "North Pacific index" after Trenberth and Hurrell 1994) for the 10 CAM3 integrations (T42 and T85 combined; top panel) and the 12 CCM3 integrations (bottom panel). Nine of the 10 CAM3 integrations exhibit negative values, with a mean of −1.92 hPa, which is close to the observed value of −2.24 hPa. In contrast, 8 of the 12 CCM3 integrations exhibit positive values, and none of the CCM3

integrations exhibits a value < −1 hPa; the mean value for the CCM3 ensemble is 0.25 hPa.

Why is CCM3 so different from CAM3 in its epoch difference atmospheric circulation response to tropical SST forcing? To gain insight into this question, we compare the simulated patterns of tropical precipitation change that force the atmospheric teleconnection to the North Pacific (Fig. 4). The tropical rainfall patterns are very similar in the two CAM3 simulations. Both exhibit the largest rainfall changes over the western two-thirds of the tropical Pacific Ocean, with positive anomalies (maximum values ~2.5–3.5 mm day^{-1}) along the equator and negative anomalies directly to the north. Negative anomalies also occur over northern South America and the adjacent Atlantic Ocean. Rainfall changes over the Indian Ocean are much weaker than those over the Pacific and are generally positive. The amplitudes of the Pacific rainfall changes are ~25% larger in the T85 version of the model compared to the T42 version, a factor that may contribute to the stronger SLP response over the North Pacific in T85 than T42.

The CCM3 tropical rainfall epoch difference simulation resembles CAM3 over the Pacific and Atlantic sectors; however, it differs greatly over the Indian Ocean where large positive values (as large as those over the equatorial Pacific) occur. CCM3 also exhibits negative rainfall changes over the far western Pacific near 15°N extending from the South China Sea to east of the Philippines, while CAM3 is weakly positive in this region.

We hypothesize that the differences between the CAM3 and CCM3 rainfall distributions over the Indian Ocean and far western Pacific may contribute to the differences in atmospheric response over the North Pacific. In particular, several modeling studies have shown that positive rainfall anomalies over the Indian Ocean west of ~110°E and negative rainfall anomalies near the Philippines force positive SLP and geopotential height anomalies over the North Pacific, opposite to the response to positive rainfall anomalies over the western and central equatorial Pacific (Branstator 1985; Ting and Sardeshmukh 1993; Barsugli and Sardeshmukh 2002; G. Branstator 2005, personal communication). Thus, we conjecture that in CCM3 the positive rainfall anomalies over the Indian Ocean (and negative rainfall changes near the Philippines) may be canceling out the effects of the positive rainfall anomalies over the equatorial Pacific in terms of their impact upon North Pacific SLP.

Before testing this hypothesis, we evaluate the realism of the simulated tropical rainfall epoch differences by comparing them to the available observational archives. As discussed in the introduction, the only direct measurements of rainfall before the satellite era are

Epoch Differences: 1977-2000 minus 1950-1976
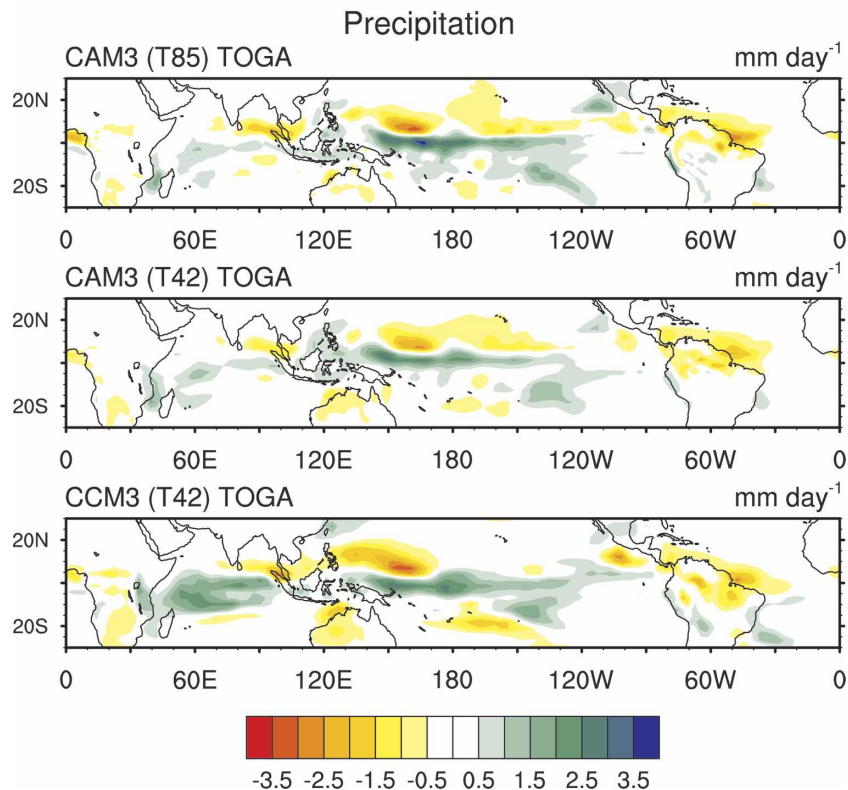### Precipitation

FIG. 4. Epoch difference maps, obtained by subtracting the period 1950–76 from the period 1977–2000, of simulated winter precipitation from the three atmospheric general circulation models forced with observed time-varying tropical sea surface temperatures (referred to as "TOGA" simulations): CAM3 at T85 horizontal resolution, CAM3 at T42 horizontal resolution, and CCM3 at T42 horizontal resolution. The color scale is given at the bottom of the figure in units of mm day^{-1}.

those at land stations: as a result, there is limited coverage over the oceans. However, indirect information on rainfall changes over the tropical oceans may be obtained from ship-based observations of cloud cover and surface wind divergence, measures closely associated with rainfall in the Tropics. Figure 5 compares epoch differences of land station rainfall from the dataset of Hulme et al. [1998; similar results are obtained using Dai et al. (1997); not shown] with those of surface wind divergence and total cloud amount from ICOADS. The land station data show rainfall increases during 1977–2000 relative to 1950–76 over the central and western equatorial Pacific (maximum values ~2.5–3.5 mm day^{-1}), flanked by decreases to the south and west. Precipitation increases are also found over Java and northwestern Australia and decreases over Malaysia, Borneo, and the Philippines. Data are sparse over the eastern Pacific, Indian, and Atlantic Oceans.

Comparison of the marine surface wind divergence and cloudiness epoch difference fields (Fig. 5, bottom)

to the land station precipitation field (Fig. 5, top) shows generally good correspondence in regions of overlapping coverage, giving confidence to the use of these measures as qualitative indicators of precipitation. In addition, the surface wind divergence and cloudiness epoch difference fields exhibit close spatial agreement and physical consistency, with areas of enhanced (diminished) cloudiness generally corresponding to regions of anomalous surface wind convergence (divergence): this agreement between two entirely independent sets of measurements strongly supports the veracity of their signals. The largest amplitude changes occur over the central equatorial Pacific, with enhanced convergence and cloudiness during 1977–2000 compared to 1950–76. [Prominent cloudiness changes in this region are also observed for the earlier North Pacific climate transitions in the 1920s and 1940s (Deser et al. 2004).] Weaker signals of enhanced convergence and cloudiness are found over the Arabian Sea and Bay of Bengal, the western half of the Indian Ocean south of

Epoch Differences: 1977-2000 minus 1950-1976

Precipitation

Cloudiness (shading) / Surface Wind Divergence (contours)

-3.5 -2.5 -1.5 -0.5 0.5 1.5 2.5 3.5 (mm day^{-1})
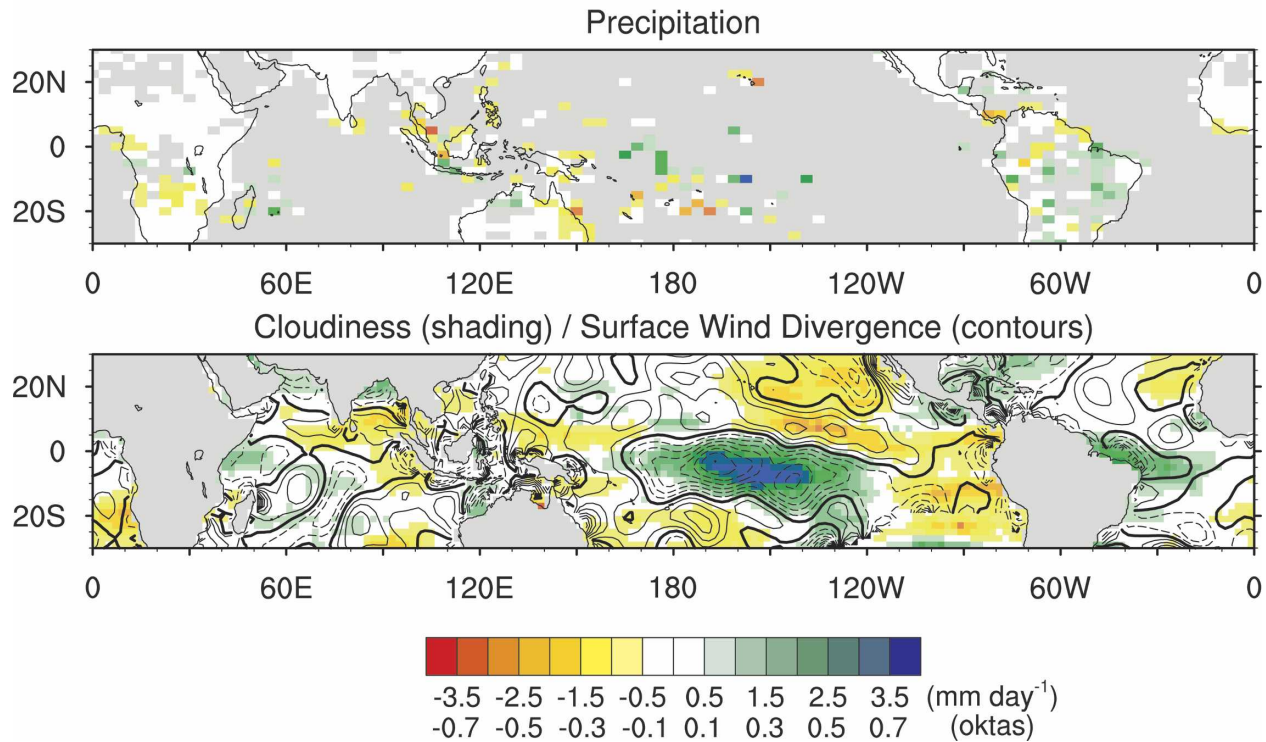-0.7 -0.5 -0.3 -0.1 0.1 0.3 0.5 0.7 (oktas)

FIG. 5. Epoch difference maps, obtained by subtracting the period 1950–76 from the period 1977–2000, of observed winter precipitation from the gridded land station dataset of Hulme et al. (1998), and of observed winter surface marine cloud amount (color shading) and wind divergence (contours) from the ICOADS dataset. The color scale is given at the bottom of the figure for both precipitation (in units of mm day^{-1}) and cloud amount (in units of oktas). The contour interval for surface wind divergence is 1×10^{-7} s^{-1}, negative contours (indicative of anomalous convergence) are dashed, and the zero contour is darkened.

the equator (albeit mixed with pockets of anomalous surface wind divergence), and the equatorial and northwestern Atlantic. Diminished cloudiness and anomalous surface wind divergence cover much of the remaining tropical oceans, especially the Indian Ocean between the equator and 10°N, the eastern Indian Ocean south of the equator, the western equatorial and southwestern tropical Pacific, and in the central Pacific along ~10°N and 160°–110°W. The regions of opposing cloudiness and surface wind divergence signals west of South and North America, where diminished cloud cover is associated with enhanced surface wind convergence, are also physically consistent as these are areas dominated by low clouds and subsidence (Klein and Hartmann 1993). In this regime, cloud cover diminishes when subsidence (and surface divergence) declines, allowing drier air to be entrained into the atmospheric boundary layer from above the low-level inversion. We note that these regions are largely nonprecipitating.

How do the simulated rainfall epoch difference maps compare with observations? In general, the primary signal of positive precipitation anomalies over the equa-

torial Pacific west of ~110°W simulated in all three models (Fig. 4) is verified in the cloudiness, divergence, and station precipitation datasets (Fig. 5), although they extend farther west in the models compared to nature. There is some observational evidence for the simulated negative rainfall anomalies directly to the north of the equator over the Pacific, although the simulated amplitudes are generally larger than observed, especially north and east of New Guinea. All three models underestimate the rainfall changes along ~20°S in the western Pacific, although CCM3 is somewhat better than CAM3 in this regard. The negative rainfall anomalies over northern South America are well simulated in all the models. While it is impossible to verify the simulated rainfall changes over the Indian Ocean with direct measurements due to lack of data, the consistent signals in cloudiness and surface wind divergence over this region suggest that the large precipitation increases over the Indian Ocean simulated in CCM3 are erroneous.

As discussed above, we wish to test the hypothesis that the different North Pacific SLP responses in CCM3

and CAM3 to tropical SST forcing associated with the 1976/77 transition are due to differences in their tropical rainfall responses. Figure 6a shows the difference between the CCM3 and CAM3 (T42) precipitation and SLP epoch difference maps. As expected from Fig. 4, there are large, widespread positive rainfall differences over the Indian Ocean and negative precipitation differences north of New Guinea. The positive rainfall differences a few degrees south of the equator in the western half of the Pacific reflect that the positive rainfall epoch differences in CCM3 extend slightly farther south than those in CAM3. The corresponding SLP differences over the North Pacific are positive, with maximum values exceeding 2.5 hPa.

To test whether the tropical precipitation differences are responsible for the North Pacific SLP differences in the CCM3 and CAM3 TOGA experiments, we have forced CCM3 with the tropical (20°N–20°S) diabatic heating epoch difference field from the ensemble mean of the CAM3 (T42) TOGA runs, and also with that from the CCM3 TOGA runs, and differenced the two experiments. Each experiment consists of adding the three-dimensional diabatic heating epoch difference anomalies to the monthly diabatic heating field from a long control run with fixed monthly mean climatological SSTs, and integrating the model for 11 yr (the last 10 yr of integration are used in our analysis). Because the model is free to adjust to the imposed diabatic heating anomalies, the equilibrium diabatic heating anomalies may differ from those initially imposed. Figure 6b shows the differences between the precipitation and SLP responses in the two CCM3 experiments (imposed CCM3 heating minus imposed CAM3 heating), scaled by 0.38. This scaling factor was obtained by taking the ratio of the area average of the absolute value of the precipitation anomalies over the tropical Indian and western Pacific Oceans (20°N–20°S, 45°–175°E) between Fig. 6a and the CCM3 heating experiment differences (imposed CCM3 heating minus imposed CAM3 heating). The scaling factor reflects that the model strongly amplifies the initial diabatic heating forcing (a similar scaling factor of 0.4 is obtained if the area averaging is computed over the entire tropical Indo-Pacific). While there is not a perfect match between the precipitation changes in Figs. 6a and 6b, there is overall agreement, with positive precipitation anomalies over the Indian Ocean and negative values over the Maritime Continent region; positive values also occur in the eastern half of the Pacific along ~5°N. The corresponding SLP response (Fig. 6b, left) closely resembles the SLP difference between CCM3 and CAM3 (Fig. 6a, left), with positive changes over the North Pacific (maximum values exceeding 2.5 hPa) and

negative changes over northeastern Siberia. The results of these experiments lend credence to the notion that disparities between the tropical precipitation epoch difference responses in CCM3 and CAM3 are responsible for differences in their North Pacific SLP responses. A caveat to this conclusion is that the precipitation differences between CCM3 and CAM3 (Fig. 6a) are not identical to those simulated by the idealized CCM3 experiments (Fig. 6b): in particular, the former exhibits weaker precipitation anomalies over the western Indian Ocean and stronger rainfall changes north of New Guinea than the latter.

To highlight the role of SSTs over the tropical Indian Ocean in forcing biases in the CCM3 tropical precipitation epoch difference response, Fig. 6c shows the mean precipitation and SLP responses from a 20-member ensemble of CCM3 forced by the observed linear trends in SSTs over the tropical Indian Ocean (25°N–25°S, 40°–110°E) from 1950 to 1999 (characterizing the SST forcing by means of linear trends or epoch differences yields nearly identical patterns; not shown). This experiment was conducted by Hoerling et al. (2004) and made available to us by the authors. As with the earlier CCM3 experiments, we have scaled the responses by the ratio (0.56) of the area average of the absolute value of the precipitation changes over the domain 20°N–20°S, 45°–175°E between Fig. 6a and the Indian Ocean SST forcing experiment. The precipitation response closely resembles that in Fig. 6b over the eastern hemisphere, indicating that positive Indian Ocean SST anomalies force both rainfall increases locally and rainfall decreases remotely over Indonesia and South Africa. In addition, the similarity of the SLP response over the North Pacific to that in Fig. 6b indicates that a substantial portion (~75%) is due to tropical precipitation changes in the eastern hemisphere associated with increased SSTs over the tropical Indian Ocean.

4. Discussion and conclusions

We have examined the contribution of tropical SST forcing to the 1976/77 climate transition of the winter atmospheric circulation over the North Pacific using a combined observational and modeling approach. We found that CAM3 (at both T42 and T85 resolutions) simulates ~75% of the observed 4 hPa deepening of the wintertime Aleutian low from 1950–76 to 1977–2000 when forced with the observed evolution of tropical SSTs, while, surprisingly, CCM3 (at T42 resolution) simulates no significant change in the strength of the Aleutian low. We traced the different atmospheric circulation responses in the two models to disparities in
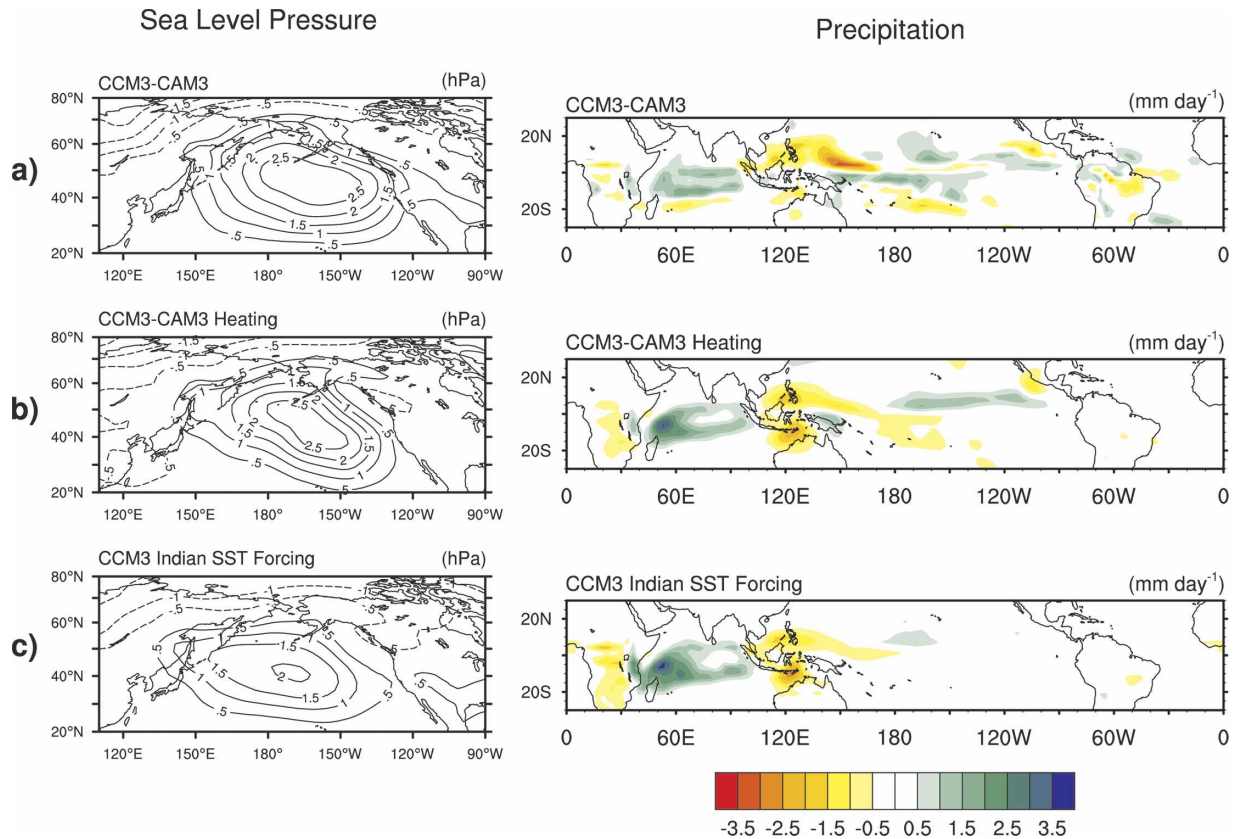
Sea Level Pressure

Precipitation

FIG. 6. (a) Difference between CCM3 and CAM3 (T42) epoch differences of winter (left) SLP and (right) precipitation. (b) Winter (left) SLP and (right) precipitation from CCM3 forced with its own tropical diabatic heating epoch difference field minus CCM3 forced with the tropical diabatic heating epoch difference field from CAM3 (T42); see text for details. (c) Winter (left) SLP and (right) precipitation responses in CCM3 forced with the observed linear SST trend from 1950 to 1999 over the tropical Indian Ocean (from Hoerling et al. 2004). The contour interval for SLP is 0.5 hPa, negative contours are dashed, and the zero contour is omitted. The color scale for precipitation is given below the right column of panels in units of mm day^{-1}.

their tropical precipitation responses. While both models exhibit similar epoch rainfall increases over the western half of the equatorial Pacific, their rainfall increases over the tropical Indian Ocean differ greatly in magnitude, with changes as large as those over the Pacific in CCM3 and much weaker anomalies in CAM3. Our estimate of the actual tropical precipitation changes associated with the 1976/77 transition, based on a combination of direct measurements at land stations and indirect information from surface marine cloudiness and wind divergence fields, compares more favorably to the CAM3 simulation than to CCM3. Based on these results, we hypothesized that CCM3's erroneously large rainfall increases over the Indian Ocean are dynamically consistent with the inability of the model to simulate the observed deepening of the Aleutian low associated with the 1976/77 transition. Further experiments aimed at testing this hypothesis confirmed that increased precipitation over the tropical Indian Ocean in CCM3 leads to reduced rainfall over

Indonesia and the far western Pacific, which together drive a positive SLP response over the North Pacific that serves to cancel the negative SLP response due to increased rainfall over the equatorial Pacific.

We have emphasized the role of tropical SST forcing (via increased rainfall over the western half of the equatorial Pacific) of the North Pacific 1976/77 climate transition. Other factors may also contribute, such as interactions between the tropically forced atmospheric circulation response over the North Pacific and the underlying oceanic mixed layer, as well as air–sea coupling within the tropical Indian and western Pacific "warm pool" regions (Alexander et al. 2002). However, the direct forcing of the 1976/77 transition in the December–February atmospheric circulation over the North Pacific by local SST changes is small according to a comparison between the TOGA ensemble and an ensemble integration forced by observed SSTs over the *global* oceans (not shown).

Not only do our observational results based on direct

and indirect measurements suggest there was no large epoch increase in rainfall over the Indian Ocean associated with the 1976/77 climate transition, but our modeling results indicate such a precipitation change would be dynamically inconsistent with the observed epoch strengthening of the North Pacific winter atmospheric circulation. Further research is needed to reconcile our findings with those of Hoerling et al. (2004) and Hurrell et al. (2004) who attribute nearly half of the recent upward trend in the winter (January–March) North Atlantic Oscillation from 1950 to 1999 to increased precipitation over the tropical Indian Ocean in response to warming of the underlying sea surface. Regardless, the demonstrated sensitivity of the global extratropical atmospheric circulation to tropical precipitation changes underscores the importance of continuing high-quality, temporally homogeneous precipitation measurements over the tropical oceans.

REFERENCES

Alexander, M. A., I. Bladé, M. Newman, J. R. Lanzante, N.-C. Lau, and J. D. Scott, 2002: The atmospheric bridge: The influence of ENSO teleconnections on air–sea interaction over the global oceans. *J. Climate,* **15,** 2205–2231.

Barsugli, J. J., and P. D. Sardeshmukh, 2002: Global atmospheric sensitivity to tropical SST anomalies throughout the Indo-Pacific basin. *J. Climate,* **15,** 3427–3442.

Branstator, G., 1985: Analysis of general circulation model sea surface temperature anomaly simulations using a linear model. Part I: Forced solutions. *J. Atmos. Sci.,* **42,** 2225–2241.

Cayan, D. R., S. A. Kammerdiener, M. D. Dettinger, J. M. Caprio, and D. H. Peterson, 2001: Changes in the onset of spring in the western United States. *Bull. Amer. Meteor. Soc.,* **82,** 399–415.

Chen, T. C., H. van Loon, K.-D. Wu, and M.-C. Yen, 1992: Changes in the atmospheric circulation over the North Pacific–North America since 1950. *J. Meteor. Soc. Japan,* **70,** 1137–1146.

Collins, W. D., and Coauthors, 2006: The Community Climate System Model version 3 (CCSM3). *J. Climate,* **70,** 2122–2143.

Dai, A., I. Y. Fung, and A. D. Del Genio, 1997: Surface observed global land precipitation variations during 1900–88. *J. Climate,* **10,** 2943–2962.

Deser, C., M. A. Alexander, and M. S. Timlin, 1996: Upper-ocean thermal variations in the North Pacific during 1970–1991. *J. Climate,* **9,** 1840–1855.

——, ——, and ——, 1999: Evidence for a wind-driven intensification of the Kuroshio Current extension from the 1970s to the 1980s. *J. Climate,* **12,** 1697–1706.

——, A. S. Phillips, and J. W. Hurrell, 2004: Pacific interdecadal climate variability: Linkages between the tropics and North Pacific in boreal winter since 1900. *J. Climate,* **17,** 3109–3124.

Dettinger, M. D., D. S. Battisti, R. D. Garreaud, G. J. McCabe Jr., and C. M. Bitz, 2000: Interhemispheric effects of interannual and decadal ENSO-like climate variations in the Americas. *Interhemispheric Climate Linkages,* V. Markgraf, Ed., Academic Press, 1–16.

DeWeaver, E., and S. Nigam, 2004: On the forcing of ENSO teleconnections by anomalous heating and cooling. *J. Climate,* **17,** 3225–3235.

Garreaud, R. D., and D. S. Battisti, 1999: Interannual and interdecadal variability of the tropospheric circulation in the Southern Hemisphere. *J. Climate,* **12,** 2113–2123.

Graham, N. E., 1994: Decadal-scale climate variability in the tropical and North Pacific during the 1970s and 1980s: Observations and model results. *Climate Dyn.,* **10,** 135–162.

——, T. P. Barnett, R. Wilde, M. Ponater, and S. Schubert, 1994: On the roles of tropical and midlatitude SSTs in forcing interannual to interdecadal variability in the winter Northern Hemisphere circulation. *J. Climate,* **7,** 1416–1441.

Hoerling, M. P., J. W. Hurrell, T. Xu, G. T. Bates, and A. S. Phillips, 2004: Twentieth century North Atlantic climate change. Part II: Understanding the effect of Indian Ocean warming. *Climate Dyn.,* **23,** 391–405.

Horel, J. D., and J. M. Wallace, 1981: Planetary-scale atmospheric phenomena associated with the Southern Oscillation. *Mon. Wea. Rev.,* **109,** 813–829.

Hulme, M., T. J. Osborn, and T. C. Johns, 1998: Precipitation sensitivity to global warming: Comparison of observations with HadCM2 simulations. *Geophys. Res. Lett.,* **25,** 3379–3382.

Hurrell, J. W., M. P. Hoerling, A. S. Phillips, and T. Xu, 2004: Twentieth century North Atlantic climate change. Part I: Assessing determinism. *Climate Dyn.,* **23,** 371–389.

Kalnay, E., and Coauthors, 1996: The NCEP/NCAR 40-Year Reanalysis Project. *Bull. Amer. Meteor. Soc.,* **77,** 437–471.

Kiehl, J. T., J. J. Hack, G. B. Bonan, B. A. Boville, D. L. Williamson, and P. J. Rasch, 1998: The National Center for Atmospheric Research Community Climate Model: CCM3. *J. Climate,* **11,** 1131–1149.

Klein, S. A., and D. L. Hartmann, 1993: The seasonal cycle of low stratiform clouds. *J. Climate,* **6,** 1587–1605.

Mantua, N., S. J. Hare, Y. Zhang, J. M. Wallace, and R. C. Francis, 1997: A Pacific interdecadal oscillation with impacts on salmon production. *Bull. Amer. Meteor. Soc.,* **78,** 1069–1079.

Miller, A. J., D. R. Cayan, T. P. Barnett, N. E. Graham, and J. M. Oberhuber, 1994: Interdecadal variability of the Pacific Ocean: Model response to observed heat flux and wind stress anomalies. *Climate Dyn.,* **10,** 287–302.

——, ——, and W. B. White, 1998: A westward-intensified decadal change in the North Pacific thermocline and gyre-scale circulation. *J. Climate,* **11,** 3112–3127.

Minobe, S., 1997: A 50–70 year climatic oscillation over the North Pacific and North America. *Geophys. Res. Lett.,* **24,** 683–686.

Nitta, T., and S. Yamada, 1989: Recent warming of tropical sea surface temperature and its relationship to the Northern Hemisphere circulation. *J. Meteor. Soc. Japan,* **67,** 375–383.

Norris, J. R., 1999: On trends and possible artifacts in global ocean cloud cover between 1952 and 1995. *J. Climate,* **12,** 1864–1870.

——, 2005: Trends in upper-level cloud cover and surface divergence over the tropical Indo-Pacific Ocean between 1952 and 1997. *J. Geophys. Res.,* **110,** D21110, doi:10.1029/2005JD006183.

Rayner, N. A., D. E. Parker, E. B. Horton, C. K. Folland, L.V. Alexander, and D. P. Rowell, 2003: Global analyses of SST, sea ice and night marine air temperature since the late nineteenth century. *J. Geophys. Res.,* **108,** 4407, doi:10.1029/2002JD002670.

Ting, M., and P. D. Sardeshmukh, 1993: Factors determining the extratropical response to equatorial diabatic heating anomalies. *J. Atmos. Sci.,* **50,** 907–918.

Trenberth, K. E., 1990: Recent observed interdecadal climate changes in the Northern Hemisphere. *Bull. Amer. Meteor. Soc.,* **71,** 988–993.

——, and D. A. Paolino, 1980: The Northern Hemisphere sea level pressure data set: Trends, errors and discontinuities. *Mon. Wea. Rev.,* **108,** 855–872.

——, and J. W. Hurrell, 1994: Decadal atmospheric–ocean variations in the Pacific. *Climate Dyn.,* **9,** 303–319.

——, G. W. Branstator, D. Karoly, A. Kumar, N.-C. Lau, and C. Ropelewski, 1998: Progress during TOGA in understanding and modeling global teleconnections associated with tropical sea surface temperatures. *J. Geophys. Res.,* **103,** 14 291–14 324.

Ward, M. N., and B. J. Hoskins, 1996: Near-surface wind over the global ocean 1949–1988. *J. Climate,* **9,** 1877–1895.

Woodruff, S. D., R. J. Slutz, R. L. Jenne, and P. M. Steurer, 1987: A Comprehensive Ocean–Atmosphere Data Set. *Bull. Amer. Meteor. Soc.,* **68,** 521–527.

——, H. F. Diaz, S. J. Worley, R. W. Reynolds, and S. J. Lubker, 2005: Early ship observational data and ICOADS. *Climatic Change,* **73,** 169–194.

Worley, S. J., S. D. Woodruff, R. W. Reynolds, S. J. Lubker, and N. Lott, 2005: ICOADS release 2.1 data and products. *Int. J. Climatol.,* **25,** 823–842.

Wu, R., and S.-P. Xie, 2003: On equatorial Pacific surface wind changes around 1977: NCEP–NCAR reanalysis versus COADS observations. *J. Climate,* **16,** 167–173.

Zhang, Y., J. M. Wallace, and D. S. Battisti, 1997: ENSO-like interdecadal variability: 1900–93. *J. Climate,* **10,** 1004–1020.

Zwiers, F. W., and H. von Storch, 1995: Taking serial correlation into account in tests of the mean. *J. Climate,* **8,** 336–351.